Astron. Astrophys. 357, 621–636 (2000)

ASTRONOMY AND ASTROPHYSICS

Internal variation of electron density in galactic HII regions

M.V.F. Copetti[1], **J.A.H. Mallmann**[1,2], **A.A. Schmidt**[1], **and H.O. Castañeda**[3]

[1] Universidade Federal de Santa Maria, Laboratório de Análise Numérica e Astrofísica, Departamento de Matemática, 97119-900 Santa Maria, RS, Brazil (mvfc@lana.ccne.ufsm.br)
[2] Universidade de Ijuí, Departamento de Física, Estatística e Matemática, 98700-000 Ijuí, RS, Brazil
[3] Instituto de Astronomía, Universidad Nacional Autónoma de México, Apartado Postal 877, BC 22860 Ensenada, México

Received 21 July 1999 / Accepted 20 March 2000

Abstract. A study on the internal variation of the electron density in galactic H II regions has been conducted on a sample of 15 objects of different sizes and evolutionary stages. The [S II] $\lambda 6716/\lambda 6731$ line ratio was adopted as electron density indicator. Long slit spectrophotometry of high signal-to-noise ratio with spectral dispersion of 0.75 Å pxl^{-1} and spatial scale of $0\farcs90$ pxl^{-1} were obtained at different slit positions and orientations. No systematic spatial variation of electron density was detected in nearly half of the objects studied (S 255, S 257, S 271, S 285, S 301, S 305, NGC 3372 and IC 1275). They are in general the most diffuse and probably evolved objects with low mean densities in the range $N_{\rm e} \approx$ 20–140 cm^{-3}. The remaining objects (S 288, S 307, NGC 2579, NGC 3503, Gum 62, Gum 64a and M 20) with mean densities $N_{\rm e} \approx$ 80–360 cm^{-3}, have shown a statistically significant electron density dependence on position. In most of these cases, the spatial variation of density may be interpreted as a radial gradient with the density decreasing from the centre to the edges. M 20 shows a systematic non-radial variation of electron density with maximum values occurring at its prominent dark lanes. A mean filling factor of the order of ϕ = 0.1 was found compatible with the data. Based on their density profiles, NGC 2579, Gum 62, Gum 64a and possibly NGC 3503 were indicated as candidates of showing a 'champagne flow'.

Key words: ISM: general – ISM: H II regions

1. Introduction

The electron density, $N_{\rm e}$, is one of the fundamental physical parameters necessary to characterise an H II region. Usually, the optical estimates of electron densities of H II regions, based on forbidden emission line ratios, are in the range 100 to 1500 cm^{-3}, well below the values of critical density of the majority of the atomic energy levels involved in the electronic transitions responsible for the observed emission-line spectra of the H II regions. So, the effects of collisional de-excitation are considered of minor importance and commonly ignored in the analysis of the observed data. This is considered to be particularly the case of most giant extragalactic objects that have mean densities of the order of $N_{\rm e} \approx 150$ cm^{-3} (McCall et al. 1985).

Usually, the density determinations published in the literature are based on data collected from few bright spots on larger nebulae or on the integrated light for smaller ones. However, since the pioneer work of Osterbrock & Flather(1959) it is known that the Orion Nebula, the prototype of a classic H II region, presents a remarkable non-homogeneous mass distribution. Based on measurements of the ratio [O II] $\lambda 3729/\lambda 3726$, they have shown the existence of a steep radial density gradient in the Orion Nebula, with the electron density decreasing from 1.8×10^4 cm^{-3} in the centre to 2.6×10^2 cm^{-3} near the edge. A similar density gradient was later found in M 8, another classic galactic H II region (Meaburn 1969). Moreover, radio techniques have revealed the existence in the Galaxy of very small and dense ($N_{\rm e} > 10^4 - 10^5$ cm^{-3}) objects, the so-called compact or ultracompact H II regions, invariably associated to regions of recent or ongoing star formation (Habing & Israel 1979). Many of these objects are optically obscure. Others are dense blobs inside extended and visible H II regions. From this considerations, we stress that single density measurements may not be representative of the whole nebula and we argue that the possibility of electron densities higher than those values usually attributed to H II regions, with important consequences on the observed spectra and on the derived chemical composition, should not be ruled out without a careful investigation. In fact, Rubin (1989) have shown by means of numerical experiments that, in the presence of a varying density, severe biases may occur in the empirical determinations of chemical abundances.

The density structure of an H II region is intimately related to its natural expansion. So, the study of electron density distribution is also important from the point of view of the dynamical evolution of the nebula. The most realistic hydrodynamical models of H II regions assume some density inhomogeneity in the surrounding molecular cloud in order to explain the usual non-spherical shapes and the kinematics of the nebulae. The successful 'blister' (Israel 1978) or 'champagne flow' (Tenorio-Tagle 1979) models are based on the idea that an expanding H II region formed near the edge of a molecular cloud will eventually break out into the less dense medium. In particular, the

Send offprint requests to: M.V.F. Copetti

development of an internal density gradient in the ionised gas is predicted in these models.

In principle, we might derive the internal distribution of the electron density within an H II region from 2D measurements of density-sensitive emission-line ratios produced by ions of different ionisation potentials assuming a geometry for the nebula. Unfortunately, only two optical line ratios, [O II] $\lambda\,3729/\lambda\,3726$ and [S II] $\lambda\,6716/\lambda\,6731$, both corresponding to low ionisation species found in the outer parts of the nebula, can be easily measured with accuracy for this purpose.

In a previous work (Castañeda et al. 1992), we have conducted a study on the spatial variation of the electron density in giant H II regions belonging to M 101, M 51 and NGC 6822, revealing the existence of systematic density variations, understood as density gradients, in many of the objects studied. Although there have been some observational works on the electron density of galactic H II region in the past, most of them were dedicated to individual objects, did not benefit from the modern detector technology, or collected data from few distinct parts of the nebulae. In the present paper, we report the results of a study on electron density variation in 15 galactic H II regions of different sizes and evolutionary stages. The electron densities were derived from the [S II] $\lambda\,6716/\lambda\,6731$ line ratios obtained from long-slit spectrophotometry at high signal-to-noise. The advantages of using this density indicator were discussed in the previous paper (Castañeda et al. 1992). Only a limited coverage of each nebula was possible due to the limitations of observing time. For this reason and to avoid unverifiable assumptions on the nebular geometry, the main objective of the present paper was to search for systematic density variations along some chosen direction over each nebula.

2. Observations and reductions

Observations were carried out on April 21–25 and November 25–27 1995 with the Cassegrain spectrograph attached to the 1.6 m telescope of the Laboratório Nacional de Astrofísica (LNA), Brazil. An EEV UV-coated CCD detector of 800×1024 pixels was used in conjunction with a 1200 grooves/mm grid yielding a dispersion of 0.75 Å pxl^{-1}. The spatial scale was $0\farcs90$ pxl^{-1}. The entrance slit used corresponded to $2\farcs5 \times 360''$ on the plane of the sky. Spectra with a resolution of 2.71 Å were obtained in the 6200–7000 Å range in order to include the H α, [N II] $\lambda\lambda\,6548, 6584$ and [S II] $\lambda\lambda\,6716, 6731$ spectral features. The observation routine followed usual procedures. Dome flat-fields exposures were taken at the beginning and at the end of the nights. About 30 bias frames were made along each night. Spectrophotometric standard stars were observed for flux calibration. Spectra of a He–Ar–Ne lamp were taken before and after each object exposure for wavelength calibration. Exposure times were limited to 20 minutes in order to reduce the effects of cosmic rays.

The objects included in this study are listed in Table 1. They have been selected to compose a sample of H II regions with a variety of sizes, surface brightness, evolutionary stages and morphologic complexity. Table 2 presents the journal of observations with the number of exposures, exposure time and slit position and orientation for each object. In general, for objects with angular diameters smaller or comparable to $6'$, the sky projected slit length, the slit was east-west oriented and centred on the central star or on the brightest central spot of the nebula. For the two largest objects of the sample, NGC 3372 (η Car Nebula) and M 20 (Trifid nebula), additional exposures were taken with different slit positions and orientations in order to improve data sampling. Multiple exposures at the same slit position were taken to increase the signal-to-noise ratio of the spectra.

The data reduction (bias correction, flat-fielding, cosmic rays cleaning, wavelength and flux calibrations, 1D spectra extraction) was carried out using the IRAF software. The spectra extracted from object frames corresponded to a rebinning of 5 CCD adjacent rows in order to increase the signal-to-noise ratio, leading to a final spatial scale of $4\farcs5$ pxl^{-1}. The fluxes of emission lines were obtained by integration of gaussian fittings. The final line fluxes were taken as the median of the flux values for each line and their error estimates as the mean absolute deviation. In the case of single observations, the uncertainties of the line fluxes were determined by Poisson statistics. The mean error in the [S II] $\lambda\,6716/\lambda\,6731$ line ratios was of the order of 3% to 4%. The effect of the interstellar extinction on the [S II] ratio is negligible, since a reddening corresponding to C(Hβ) = 3.0, higher than those found in the literature for the studied objects (see Table 1), would require, according to the usual laws of galactic extinction, a correction of 1%.

3. Determination of the electron density

The electron densities determinations were obtained from the [S II] $\lambda\,6716/\lambda\,6731$ line ratios by solving numerically the equilibrium equations for a five-level atom approximation using the FIVEL program (De Robertis et al. 1987). The energy levels, transition probabilities and collisional strength values for the [S II] ion were taken respectively from Bowen (1960), Keenan et al. (1993) and Ramsbottom et al. (1996). The electron density $N_{\rm e}$ derived from the observed [S II] line ratio depends on the electron temperature T_e assumed for the nebula. However, this dependence of $N_{\rm e}$ on the T_e is weak for the range of electron temperatures usually found in galactic H II regions. Table 3 lists the values of the electron temperature found in the literature and the adopted values for this work. For the objects with no electron temperature measurements, a mean estimate based on the correlation between the electron temperature and the galactocentric distance of the nebula has been adopted.

The [S II] line ratio is a reliable indicator of the electron density in the range 200 cm$^{-3} < N_{\rm e} < 5\,000$ cm^{-3}. However this line ratio saturates at both lower and higher values of the electron density what makes the usage of the [S II] line ratio unsuitable for electron densities $N_{\rm e} < 20$ cm^{-3} or $N_{\rm e} > 30\,000$ cm^{-3}. This is the most significant source of error in the electron density evaluation for galactic H II regions.

Table 1. Selected objects

Object	l	b	D (kpc)		R (kpc)	Size ($'$)	d (pc)	C(Hβ)	Other names
S 255	192.°63	-0.°02	2.5 ± 0.4	[1,2]	11.0	3.6×4.0	2.8	1.6 [18,19,20]	IC 2162
S 257	192.58	-0.08	2.5 ± 0.4	[1,2]	11.0	3.0×3.8	2.5	1.7 [18,19,20]	
S 271	197.78	-2.32	4.8 ± 0.5	[1]	13.1	1.9×1.6	2.5	1.7 [18,21,22]	PK 197-02 1, V-V 1-4
S 285	213.83	0.62	6.7 ± 0.3	[1,3,4]	14.5	1.7×1.7	3.3	1.3 [18,22]	
			4.3 ± 0.3	[5,6]	12.3		2.1		
S 288	218.74	1.85	3.0 ± 1.2	[1]	11.0	1.4×1.7	1.4	1.3 [18]	WB89 952
S 301	231.49	-4.40	5.9 ± 0.2	[1,3]	13.0	8×7	13	1.0 [22]	Gum 5, RCW 6
S 305	233.76	-0.19	5.4 ± 0.3	[1,4]	12.5	3.0×4.2	5.7	1.9 [18]	RCW 8
S 307	234.58	0.84	2.2 ± 0.5	[1]	9.9	3.7×3.7	2.4	1.6 [18]	Gum 7, RCW 12
			4.2 ± 0.5	[7]	11.5		4.5		
NGC 2579	254.68	0.22	3.4	[8]	10.0	2×2	2.0	0.2 [9]	Gum 11, RCW 20
			1.3	[9]	8.9		0.8		
NGC 3372	316.83	0.09	2.6 ± 0.2	[10,11,12]	6.8	120×120	91	0.7 [20,23]	Carina Neb., Gum 33, RCW 53
NGC 3503	289.51	0.12	2.8 ± 0.3	[13]	8.0	3×3	2.4	0.7 [13]	
Gum 64a	351.16	0.67	2.0 ± 0.3	[12,14]	6.5	2×2	1.2	1.7 [12,14]	NGC 6334, RCW 127, S 8
Gum 62	351.21	0.47	2.0 ± 0.3	[12,14]	6.5	8×8	4.7	1.7 [12,14]	NGC 6334, RCW 127, S 8
M 20	7.00	-0.26	1.8 ± 0.3	[11,15,16]	6.7	29×27	15	0.5–1.8 [24]	Trifid nebula, NGC 6514
IC 1275	7.22	-2.16	1.4 ± 0.4	[17]	7.1	10×6	3.3	0.5 [17]	

References: [1] Moffat et al. (1979); [2] Pişmiş & Hasse (1976); [3] Lahulla (1987); [4] Turbide & Moffat (1993); [5] Rolleston et al. (1994); [6] Smartt et al. (1996); [7] Russeil et al. (1995); [8] Neckel & Staude (1995, for RCW 19/20); [9] Janes & Adler (1982); [10] Tapia et al. (1988); [11] Walborn (1973); [12] Walborn (1982); [13] Herbst (1975); [14] Neckel (1978); [15] Buscomb (1963); [16] Lada & Wooden (1979); [17] Herbst et al. (1982, for Simeis 188); [18] Hunter (1992); [19] Matthews (1981); [20] Shaver et al. (1983); [21] Chopinet & Lortet-Zuckermann (1976); [22] Fich & Silkey (1991); [23] Peimbert et al. (1978); [24] Lynds et al. (1985);
Conventions: l, b: galactic coordinates, in degree; D: distance from the Sun; R: galactocentric distance; d: mean diameter; C(Hβ): logarithmic extinction in Hβ.
Catalogues: Gum = Gum (1955); PK = Perek & Kohouteck (1967); RCW = Rodgers et al. (1960); S = Sharpless (1959); V-V = Vorontsov-Velyaminov (1953); WB89 = Wouterloot & Br and (1989).

4. Results

The obtained spatial profiles along the slit of the Hα flux, the [S II] $\lambda 6716/\lambda 6731$ line ratio and the derived electron density are shown in Figs. 1–21. Table 4 presents some nonparametric statistics of the [S II] ratio and the electron density measurements, including the number N of distinct nebular areas, the median, the first and third quartiles, Q1 and Q3 respectively, the limits between which 50% of the values lie, the minimum [S II] ratio and the corresponding maximum density.

In order to check our results, we have searched in the literature for electron density measurements for the observed objects. In special, Hunter (1992) have measured the [S II] doublet in 3 to 10 different areas throughout each of the Sharpless objects of our sample but S 301. The [S II] ratios from this paper are in general similar to our values for common nebular areas. However, the densities derived by Hunter (1992) are higher than ours by a factor of 2 to 5. Only a small part of this discrepancy is due to the adoption of different values of electron temperature. So, the difference must be accounted on the use of out-of-date atomic parameters. In fact, the calibration of electron density with the [S II] $\lambda 6716/\lambda 6731$ line ratio have been significantly changed over the years (see McCall 1984, Castañeda et al. 1992). For instance, according to Saraph & Seaton (1970), at an electron temperature of 10 000 K, [S II] $\lambda 6716/\lambda 6731 = 1$ would correspond to $N_{\rm e}$ = 2200 cm^{-3}, while the current evaluation would be of $N_{\rm e}$ = 610 cm^{-3}. Therefore, whenever the [S II] ratios were available we have compared them directly with our values or rederived the corresponding electron densities using the same atomic parameters and electron temperature adopted in the present paper.

In the following, the observed objects are discussed separately.

4.1. S 255 and S 257

These objects form with S 254 and S 256 a close group of small and nearly spherical H II regions (see Israel 1976). S 255 and S 257 are similar in size and morphology. Both objects show irregularities in their Hα and Hβ brightness distributions (Hunter 1992; Chopinet et al. 1974) not reproduced in their radio maps (Israel 1976; Fich 1993; Turner & Terzian 1985) due to the presence of extensive dark lanes over parts of the nebulae. In particular, S 255 can be divided in two halfs, with the north-eastern part much brighter than the south-western one (Chopinet et al. 1974). S 255 and S 257 present a very homogeneous electron density distribution (see Figs. 1, 2 and 3), with mean densities of $N_{\rm e} = 138^{+21}_{-10}$ cm^{-3} and $N_{\rm e} = 119^{+19}_{-45}$ cm^{-3}, respectively. Statistically, we can say that the obtained values of density are constant within a level of confidence of 90%.

Chopinet et al. (1974) have measured the electron density distribution from [S II] along a direction close the east-west one

Table 2. Journal of observations

Object	slit centre			PA[a]	exposure time (s)
	α (2000)	δ (2000)	offset		
S 255	$06^{\rm h}13^{\rm m}04.2^{\rm s}$	$17^\circ58'41''$		90°	3×1200
	06 13 04.2	17 58 23	18″S	90	3×1200
S 257	06 12 44.2	17 59 14		90	1×1200
S 271	06 14 53.3	12 21 24		90	3×1200
S 285	06 55 16.9	−00 31 17		90	1×1200 + 2×600
S 288	07 08 39.2	−04 19 01		90	4×1200
	07 08 39.2	−04 19 01		134	1×1200
S 301	07 09 55.2	−18 30 08		90	1×1200
S 305	07 30 06.1	−18 32 19		90	1×1200 + 1×900
S 307	07 35 34.1	−18 45 34		90	3×1200
NGC 2579	08 20 54.8	−36 13 00		90	1×800 + 4×1200
NGC 3372	10 45 03.8	−59 36 06	5′N	90	2×1200
	10 45 03.8	−59 31 06	10′N	90	2×1200
	10 45 03.8	−59 26 06	15′N	90	2×1200
	10 45 03.8	−59 16 06	25′N	90	1×1200
	10 45 03.8	−59 06 06	35′N	90	1×1200
	10 45 03.8	−59 36 06	5′N	0	3×1200
	10 45 03.8	−59 31 06	10′N	0	2×1200
	10 45 03.8	−59 26 06	15′N	0	2×1200
	10 45 03.8	−59 21 06	20′N	0	1×1200
	10 45 03.8	−59 16 06	25′N	0	1×1200
	10 45 03.8	−59 11 06	30′N	0	1×1200
NGC 3503	11 01 19.0	−59 50 57		90	3×1200
Gum 64a	17 20 03.3	−35 58 25		90	3×1200
Gum 62	17 21 00.5	−36 03 30		90	3×1200
M 20	18 02 23.1	−23 01 59		90	3×1200
	18 02 23.1	−23 01 59		18	3×1200
	18 02 23.1	−23 01 59		160	1×900 + 1×600
	18 02 23.1	−23 01 34	25″N	90	3×1200
IC 1275	18 10 06.8	−23 46 22		90	3×1200 + 1×900

[a] PA: position angle.

(more precisely, PA = 80°) for S 255 and along the north-south direction for S 257. Although their higher densities up to near 2000 cm^{-3} are brought closer to our values with the use of up-to-date atomic parameters, the systematically higher densities in the more obscured (western) part of S 255 and the association of density peaks with regions of abrupt brightness variations reported by Chopinet et al. (1974) were not corroborated by our homogeneous data. Hunter (1992) have also obtained relatively constant [S II] rations from 10 different areas of S 255 and from 5 areas of S 257, with mean values of 1.24 ± 0.07 and 1.31 ± 0.03 respectively, which are entirely compatible with our values (see Table 4). So, we conclude that the much higher electron densities derived in these two papers are a consequence of the use of out-of-date atomic parameters. Although there are many signs of recent star formation in the molecular cloud associated with these H II regions, they come mainly from the area between S 255 and S 257 (Israel 1976). The evidence of an extended dust depletion zone in the central part of each nebulae indicates that they are relatively evolved objects (Nakano et al. 1983).

4.2. S 271

This object has been misclassified as planetary nebula (Sabbadin & Hamzaoglu 1981; Zijlstra et al. 1990). S 271 is similar in size, surface brightness and morphology to S 255 and S 257: it has a spherical shape, very symmetric in radio maps (Albert et al. 1986; Fich 1993) but with extended dark areas on optical images (Hunter 1992). Fig. 4 shows a uniform distribution of density with a mean value of $N_{\rm e} = 110^{+52}_{-28}$ cm^{-3}. No trace of very young sources was ever detected towards S 271 (Lo & Burke 1973; Persi et al. 1987), indicating that this is also an evolved object.

4.3. S 285

This objects has a low surface brightness and a roughly round shape with a diffuse halo to the south (Fich 1993; Hunter 1992). The data obtained for S 285 (see Fig. 5) is consistent with an homogeneous low density of $N_{\rm e} = 41^{+47}_{-41}$ cm^{-3}, in accordance with the findings of Hunter (1992), Fich & Silkey (1991) and

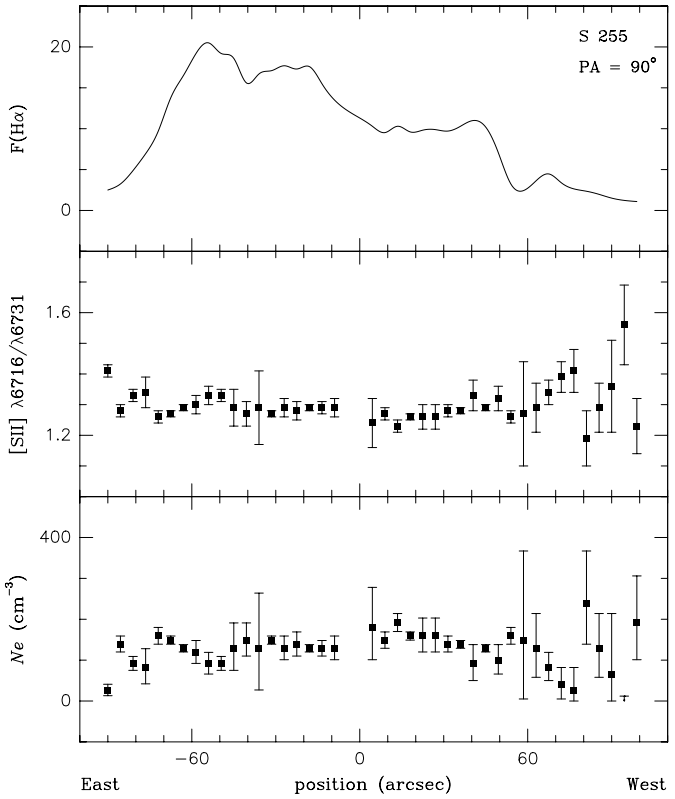

Fig. 1. S 255. Spatial profiles along the slit of the Hα flux (in units of 10^{-14}ergs cm^{-2} s^{-1}), the [S II] $\lambda\,6716/\lambda\,6731$ line ratio and the derived electron density. The position is relative to the slit centre shown in Table 2. Position angle PA = 90° corresponds to east-west orientation

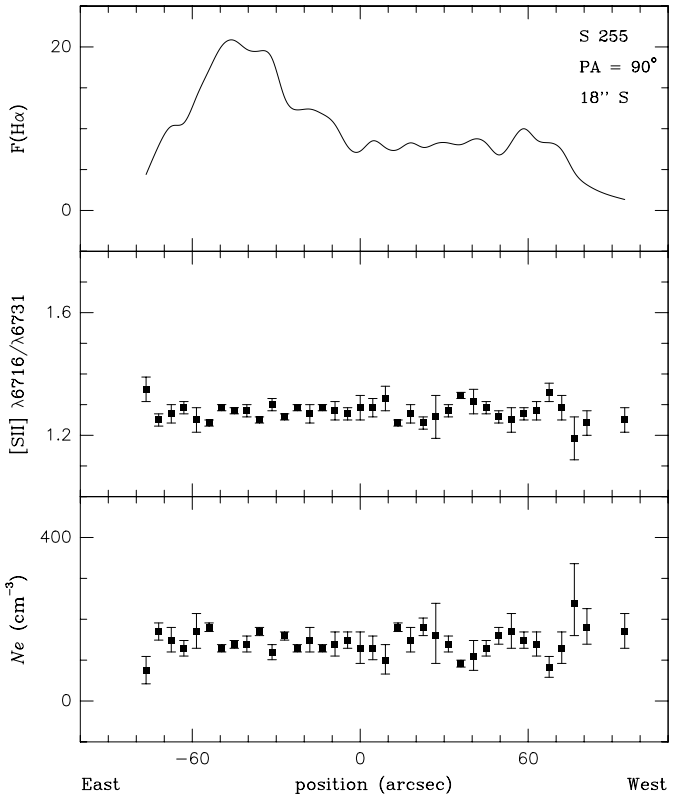

Fig. 2. S 255, $\Delta\delta$ = 18″S. Same as Fig. 1 but with the slit shifted 18″ towards the south

Vílchez & Esteban (1996) that the [S II] ratio is close to the low-density limit. Kilian-Montenbruck et al. (1994) and Rolleston et al. (1994) have estimated ages from 3 to 9 $\times 10^6$ years for two stars in the ionising cluster of S 285. Based on isochrone fitting Turbide & Moffat (1993) have obtained an estimate around 6×10^6 years for the age of this stellar group.

4.4. S 288

This is a bright and small nebula, with a spherical morphology in radio (Fich 1993). An obscured area to the west of the centre and some bright rims are visible on the red Palomar Observatory Sky Survey (POSS) prints. S 288 presents a systematic density variation, with the electron density ranging from 100 cm^{-3} to 700 cm^{-3}. The density profile along the east-west direction (Fig. 6) peaks 14″ to the west of the Hα brightness maximum, close to the obscured area, and decreases outwards. The density distribution along the south-east orientation (PA = 134°, Fig. 7) is more complex, with the electron density showing two local peaks 14″ away from the Hα maximum, at both sides, and a third peak on the bright rim located to the north-west of the nebula. From the [O III] $\lambda\,52\,\mu$m/$\lambda\,88\,\mu$m line ratio Rudolph et al. (1997) have derived an electron density of $N_{\rm e} = 320^{+160}_{-110}$ cm^{-3}. We remark that this density estimate for the doubly ionised oxygen zone

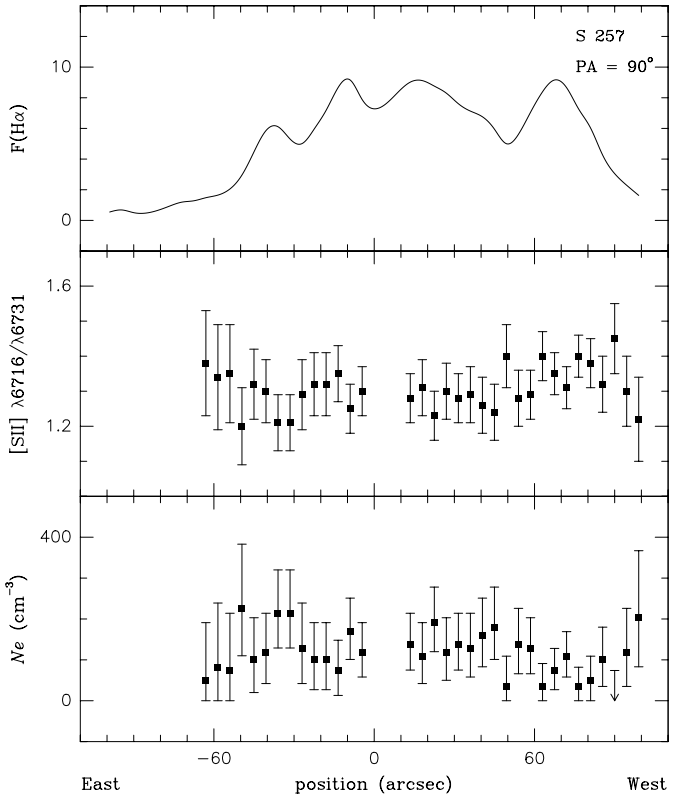

Fig. 3. S 257. Same as Fig. 1

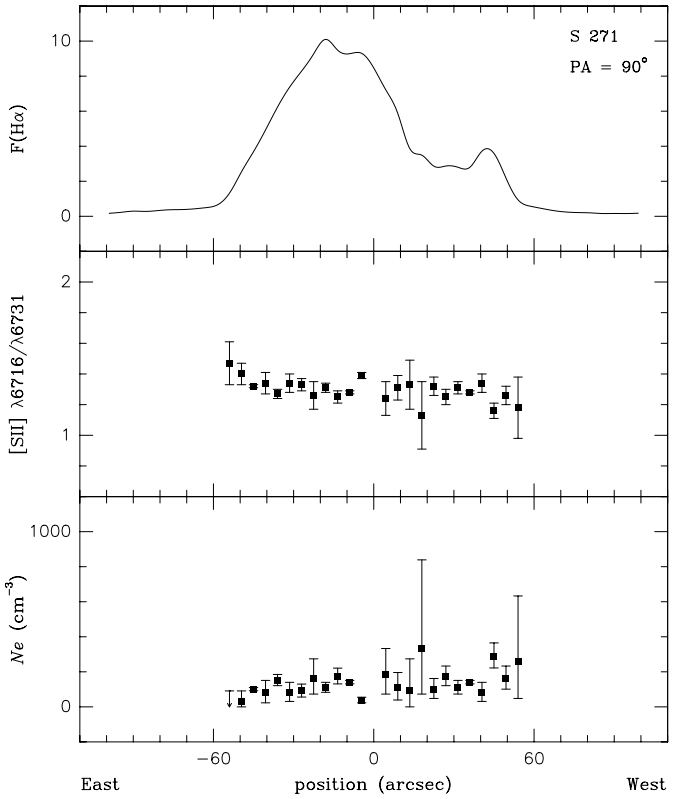

Fig. 4. S 271. Same as Fig. 1

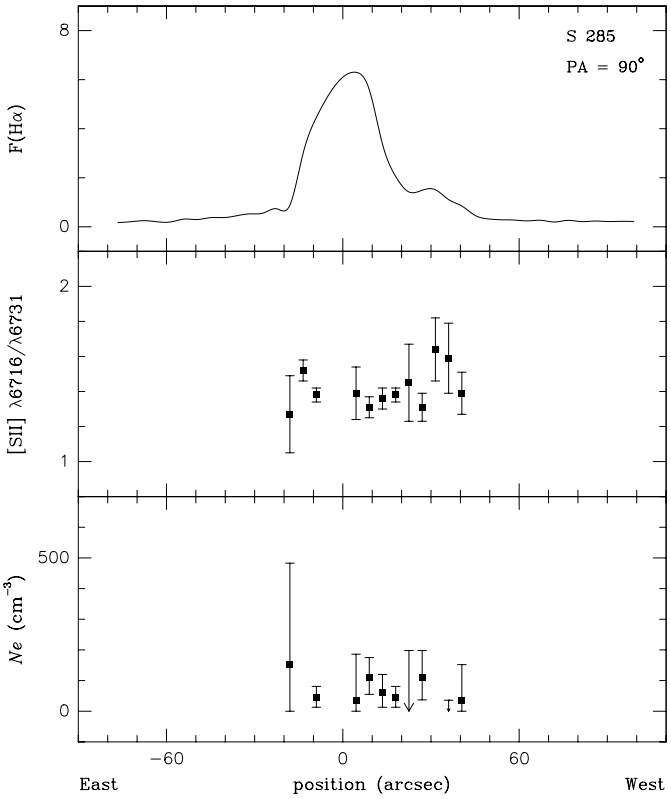

Fig. 5. S 285. Same as Fig. 1

indicates that very high densities are not expected in the inner parts of S 288. The density values up to 5000 cm^{-3} attributed by Hunter (1992) to S 288 are, according to the up-to-date atomic data, incompatible with her own [S II] line ratio measurements.

4.5. S 301

This is a diffuse object with a complex morphology and a low surface brightness. With a diameter of 13 pc, close to that of M 20, this nebula has an intermediate size in our sample. The densities obtained in the present work for S 301 are homogeneously low with a mean value of $N_{\rm e} = 25^{+31}_{-25}$ cm^{-3}. Fich & Silkey (1991) have measured the [S II] line ratio over the low density limit. The lack of signs of recent star formation indicates that this is an old H II region.

4.6. S 305

S 305, S 307 and possibly S 301 are associated to a same molecular cloud complex (Russeil at al. 1995). In Hα this object has low surface brightness and irregular shape, with an extended and diffuse halo to the south (Hunter 1992). On the 1465 MHz map of Fich (1993) this object shows a cometary morphology. This morphology and the negative radial velocity difference between the ionised and molecular material were considered by Russeil et al. (1995) as indications of a 'champagne effect' (Tenorio-Tagle 1979) in S 305. However, Turbide & Moffat (1993) have derived an age of 6×10^6 years for the ionising cluster of S

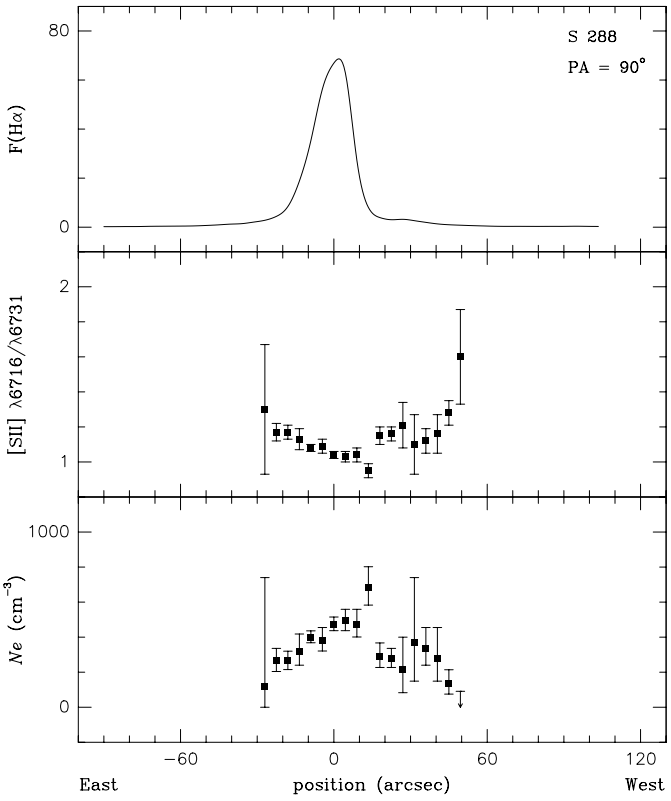

Fig. 6. S 288, PA = 90°. Same as Fig. 1

Table 3. Electron temperatures.

	Literature			Adopted
Object	T_e (K)	method	ref.	T_e (K)
S 255	8300	[NII]	[1]	8000
	5550	H109α	[2]	
	5900	H137β	[2]	
	9600	H167α	[3]	
	9900	H140α	[3]	
S 257	< 9300	[NII]	[1]	8000
	7100	H167α	[3]	
	7000	H140α	[3]	
S 271				9000
S 285				9500
S 288				8000
S 301	7700		[4]	8400
S 305				8500
S 307	7400	H109a	[5]	8000
NGC 2579				7500
NGC 3372	9000	[OIII], [NII]	[1]	8900
	8800	[OIII], [NII]	[6]	
	5000	H166α	[7]	
	7700	H76α	[8]	
NGC 3503				7000
NGC 6334	5700	H166α	[9]	7000
	6400	H109α	[10]	
	7200	H76α	[10]	
	6100	H109α	[11]	
	6400	H109α	[12]	
	6770	H76α	[8]	
M 20	8800	[NII]	[13]	8800
	8150	H110α	[14]	
IC 1275				6500

References: [1] Shaver at al. (1983); [2] Kazes et al. (1977); [3] Silverglate & Terzian (1979); [4] Felli & Churchwell (1972); [5] Caswell & Haynes (1987); [6] Peimbert et al. (1978); [7] Azcarate et al. (1990); [8] McGee & Newton (1981); [9] Azcarate et al. (1987); [10] Azcarate (1991); [11] Wilson et al. (1970); [12] Reifenstein et al. (1970); [13] Hawley (1978); [14] Chaisson & Willson (1975).

305, indicating that this in an evolved object. The best known candidates of 'blister' (Israel 1978) or 'champagne flow' configuration (e.g. the Orion Nebula) are much younger H II regions. Fig. 9 shows that the electron density is relatively homogeneous in S 305 with a mean value of $N_{\rm e} = 91^{+29}_{-42}$ cm^{-3} except for a density peak reaching $N_{\rm e} = 485 \pm 60$ cm^{-3} on the western side of the nebula.

4.7. S 307

On the red POSS print this object appears as a half-shell surrounded by fainter emissions to the west. The radio morphology resembles well the optical structure (Fich 1993). The density profile along the east-west orientation obtained for S 307 (Fig. 10) shows a well defined spatial variation of the electron density with a peak of $N_{\rm e} = 485 \pm 60$ cm^{-3} at brightest point about 8 times denser that the outer areas. Although the [S II]

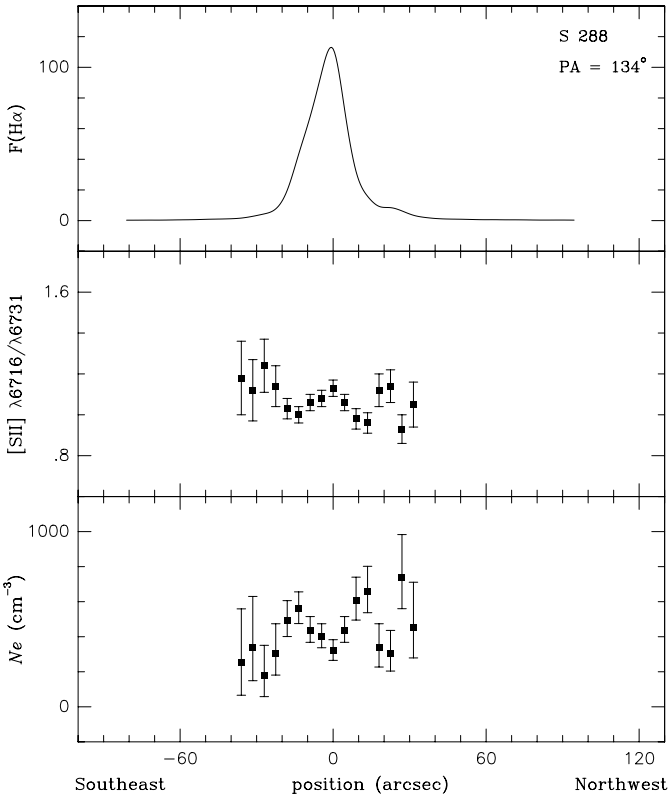

Fig. 7. S 288, PA = 134°. Same as Fig. 1

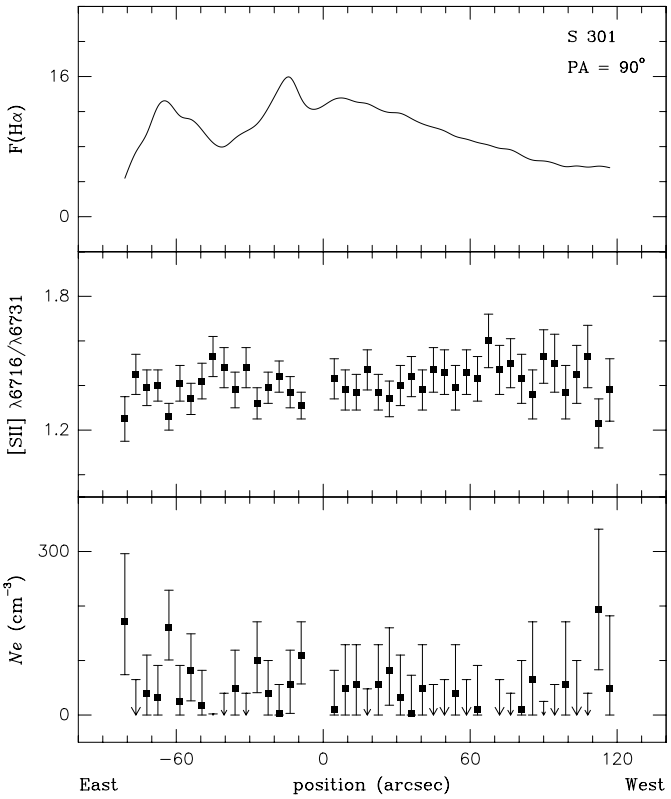

Fig. 8. S 301. Same as Fig. 1

Table 4. [S II] ratio and electron density statistics.

		[S II] $\lambda 6716/\lambda 6731$				N_e (cm^{-3})			
Object	N	Q1	Median	Q3	Minimum	Q1	Median	Q3	Maximum
S 255	78	1.26	1.28	1.29	1.19±0.07	128	138	159	239^{+97}_{-79}
S 257	34	1.28	1.30	1.35	1.20±0.11	74	119	138	226^{+157}_{-116}
S 271	24	1.26	1.31	1.34	1.13±0.22	82	110	162	333^{+506}_{-260}
S 285	12	1.34	1.39	1.49	1.27±0.22	0	41	86	152^{+331}_{-152}
S 288	36	1.04	1.12	1.17	0.93±0.07	271	336	474	740^{+243}_{-180}
S 301	43	1.37	1.41	1.47	1.23±0.11	0	25	56	193^{+148}_{-110}
S 305	32	1.30	1.33	1.38	1.04±0.03	49	91	120	485^{+63}_{-57}
S 307	37	1.22	1.27	1.40	0.98±0.01	34	148	203	606^{+24}_{-23}
NGC 2579	32	0.99	1.10	1.18	0.73±0.02	253	359	559	1709^{+182}_{-157}
NGC 3372	958	1.34	1.37	1.39	1.10±0.02	39	55	82	380^{+35}_{-32}
NGC 3503	40	1.30	1.34	1.36	1.26±0.02	66	82	116	154^{+52}_{-45}
Gum 64a	44	1.11	1.14	1.21	1.01±0.02	206	286	335	510^{+43}_{-39}
Gum 62	36	1.12	1.17	1.20	1.02±0.02	218	254	320	490^{+41}_{-38}
M 20	172	1.21	1.26	1.30	1.13±0.02	125	161	213	330^{+32}_{-29}
IC 1275	41	1.40	1.43	1.46	1.36±0.04	0	17	37	66^{+32}_{-28}

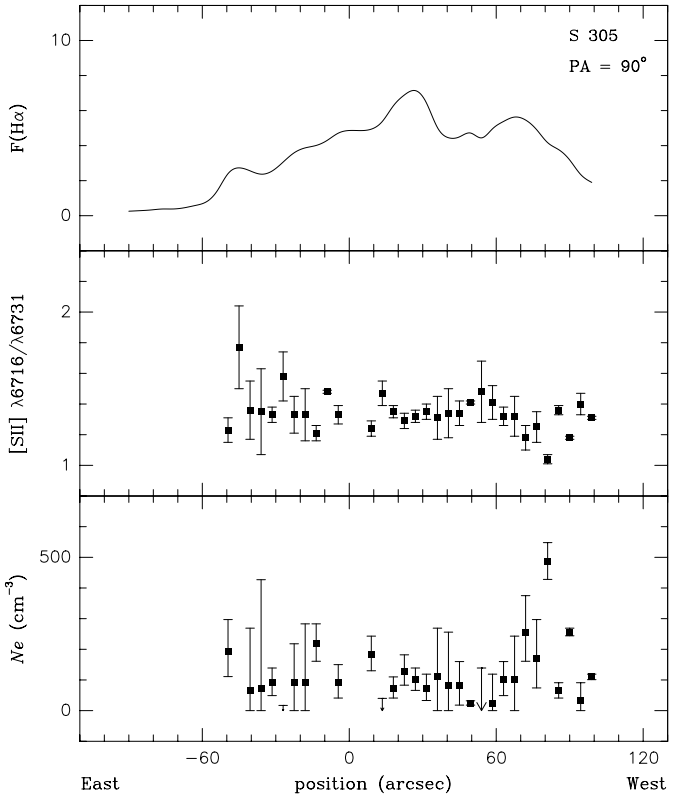

Fig. 9. S 305. Same as Fig. 1

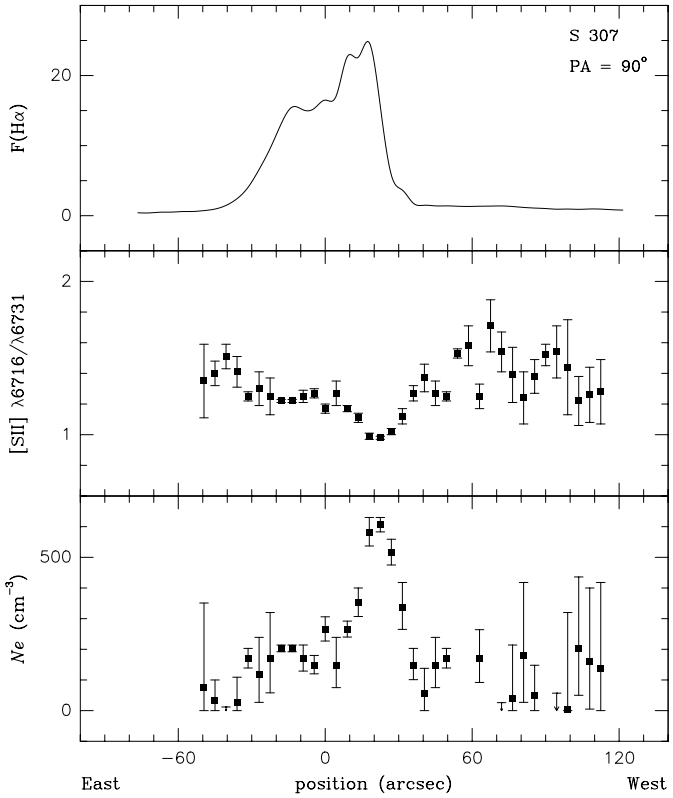

Fig. 10. S 307. Same as Fig. 1

ratios obtained by Hunter (1992) are comparable with our measurements, the densities derived by her are up to 5 times higher. Due to the asymmetrical morphology of the nebula, its position close to a CO peak, the negative difference between the Hα and CO velocities and its high rms electron density there have been some suggestions in the literature that S 307 is exhibiting a 'blister' or a 'champagne flow' effect (Albert et al. 1986; Felli & Harten 1981; Russeil et al. 1995). This indication is strongly supported by the electron density gradient revealed in the present work, since this density structure is naturally predicted by the 'champagne model'. Persi et al. (1987) have not found any evidence of very young objects associated to S 307.

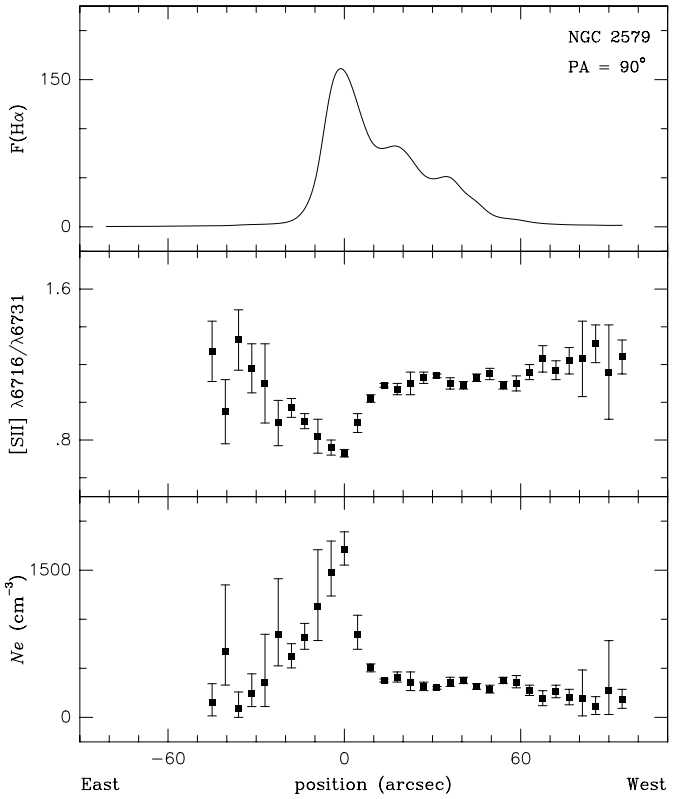

Fig. 11. NGC 2579. Same as Fig. 1

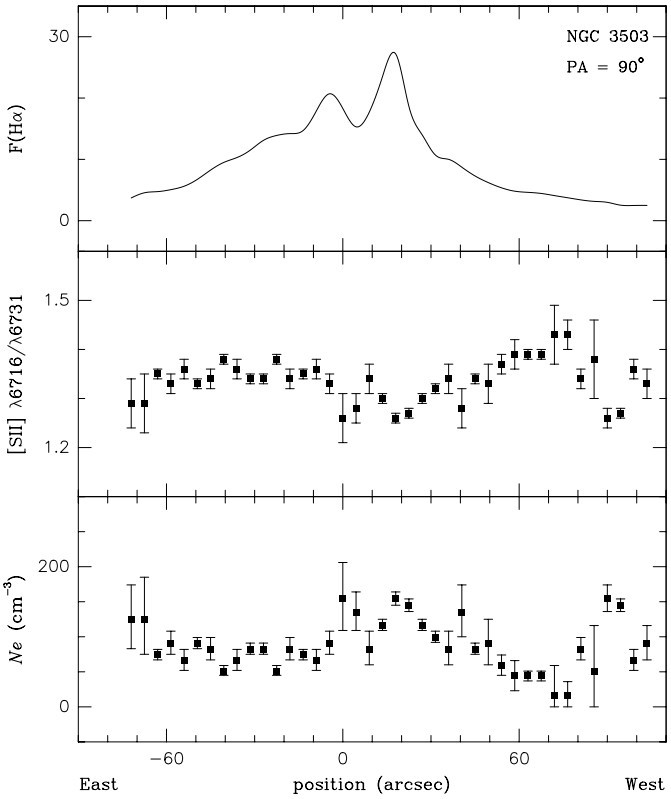

Fig. 12. NGC 3503. Same as Fig. 1

4.8. NGC 2579

NGC 2579 = Gum 11 is some times identified as RCW 20 (see the comparison catalogue of Maršálková 1973). However, NGC 2579 is properly the object that appears on Hα images (Lyngå & Hansson 1972) as a small and bright blob 20′ towards the east of RCW 20. On the other hand, it is probably physically associated with the nebular complex RCW 19/20. Our observations have revealed a strong density gradient in NGC 2579 (Fig. 11) with the electron density increasing from $N_{\rm e} \approx 100$ cm^{-3} at the outskirts of the nebula to the peak value $N_{\rm e} = 1709^{+182}_{-157}$ cm^{-3} at brightest part. This is the densest object in our sample. Unfortunately this interesting object has been poorly studied. Although we have not found in the literature any reference on the dynamics of this nebula, we suspect that it is a very good candidate of exhibiting a 'champagne flow'.

4.9. NGC 3503

This small and bright nebula ionised by the compact star cluster Pis 17 is located towards the centre of RCW 54, a 210′× 60′ nebula. The data obtained for NGC 3503 (Fig. 12) show a clear variation of the electron density with position along the east-west orientation with two density peaks reaching $N_{\rm e} = 154 \pm 53$ cm^{-3} at the two Hα maxima close to the centre of the nebula and a third peak 90″ to the west.

4.10. NGC 3372 – The η Carina nebula

The η Carina nebula is considered one of the giant H II regions of the Galaxy. In deep Hα exposures this nebula seems to extend over a region of 300 pc in diameter (Kennicutt 1984). Due to the large angular size of this object, we were only able to get a very limited covering of the whole nebula. All our data were collected from areas to the north of the η Car star located at the centre of the nebula. The slit was centred at 7 equally spaced positions, 5′ apart, along the hour circle crossing η Car. A number of exposures with the slit orientated along the east-west and south-north directions were taken (see Table 2). Many of the brightest parts of the nebula are outside the areas studied. Fig. 13 shows the spatial variation of the Hα flux, the [S II] ratio and the derived electron density along the south-north direction. Except for two density peak of $N_{\rm e} \approx 350$ cm^{-3} and $N_{\rm e} \approx 380$ cm^{-3} at the position 519″ and 1272″ respectively, probably associated with bright filaments, only a slight modulation of the electron density with position is shown in this figure. The density values measured from the exposures taken with east-west slit orientation (transversal to the radius of the nebula) at 5 different distances from η Car (Fig. 14) are remarkably uniform. We have found a very low mean electron density of $N_{\rm e} = 55^{+27}_{-16}$ cm^{-3} for this nebula.

Peimbert et al. (1978) have measured the electron density in 6 different points on the bright area not covered by our observation in the vicinity of centre of the Car II radio source 3′ to the north-west of η Car (see Deharveng & Maucherat 1975). From

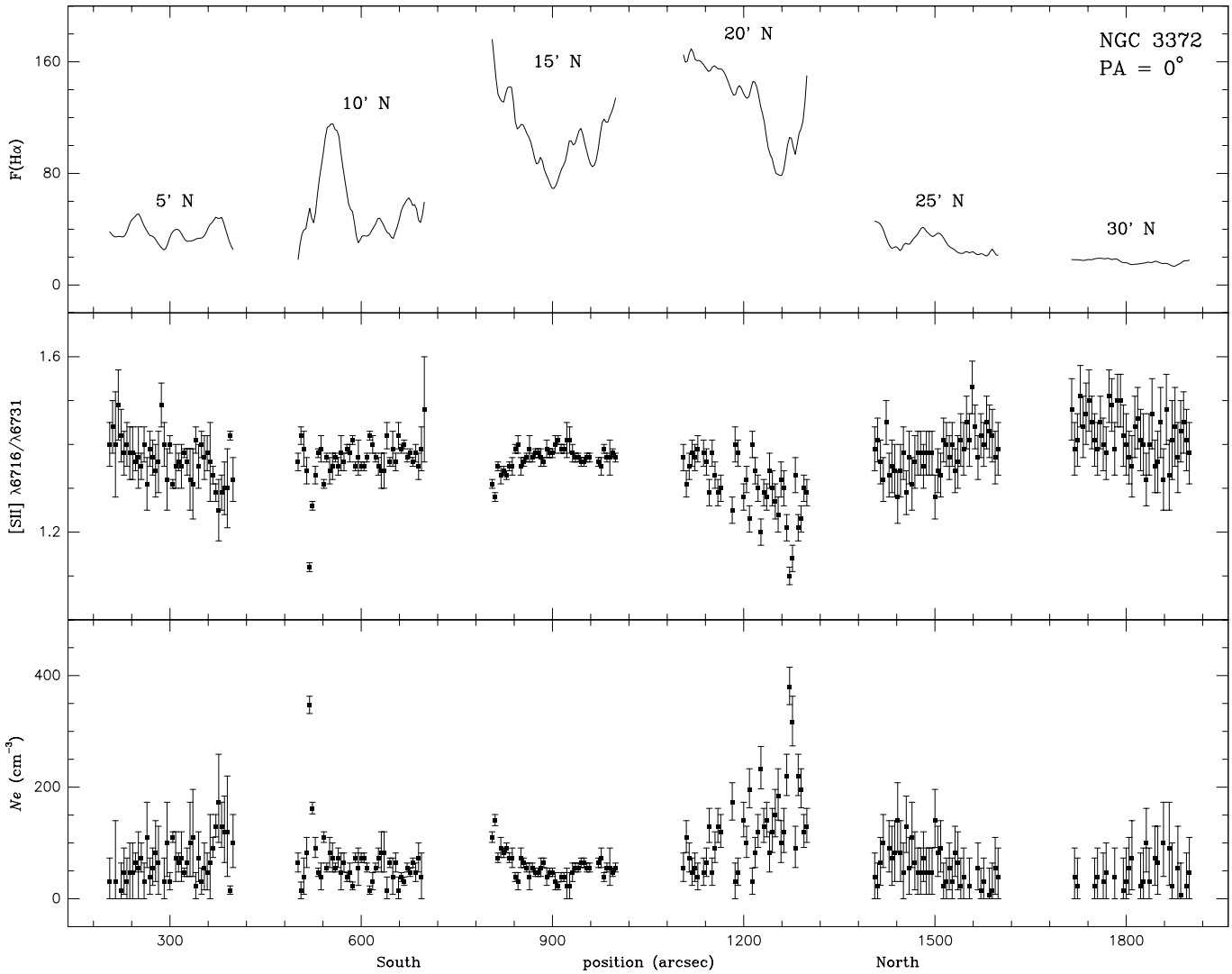

Fig. 13. NGC 3372 – The η Carina nebula, PA = 90°. South-north data profiles along the hour circle crossing η Car. Positions are relative to this star. The labels are the offsets in declination of the slit centre from this star. Other conventions as in Fig. 1

their [S II] ratios we have recalculated the electron densities using updated atomic data, and we have derived values ranging from 23 to 581 cm^{-3}.

From a azimuthally averaged emission-measure profile obtained from radio continuum data Kennicutt (1984) have indicated the existence of a steep radial gradient of the rms electron density in the η Carina nebula with the density decreasing away from the centre. One way to reconcile this conclusion with the relatively homogeneous forbidden-line densities measured in the present work would be to assume a radial decrease of the filling factor in this nebula. Alternatively, if a nebula with constant electron density has a shape elongated along the line of sight, a brightness profile deconvolution based on the assumption of spherical symmetry similar to that performed by Kennicutt (1984) would produce a rms density profile with a radial gradient. However, we believe that the latter explanation, valid in principle, is unrealistic for the case of the Carina nebula, a giant H II regions with a diameter around 100 pc, since it would require an unreasonable deepness for the nebula of the order of kiloparsecs.

The Carina region presents one of the largest concentration of early-type stars in the Galaxy with more than 60 O-type stars detected. The open clusters embedded in the Carina nebula have age estimates ranging from 3 to 7 $\times 10^6$ years (Feinstein 1995).

4.11. Gum 62 and Gum 64a in NGC 6334

On Hα images NGC 6334 = RCW 127 appears as a group of distinct H II regions (Walborn 1982). Radio observations of the region reproduce well the optical morphology (Shaver 1969; Rodríguez et al. 1982). On longer exposures the whole area of about $1^\circ \times 1^\circ$ is filled with Hα emission (Georgelin & Georgelin 1970), indicating a physical association among these objects. The bright H II regions are separated by dense and dusty molecular clouds. The considerable number of compact infrared and radio sources, ultra-compact H II regions, OH,

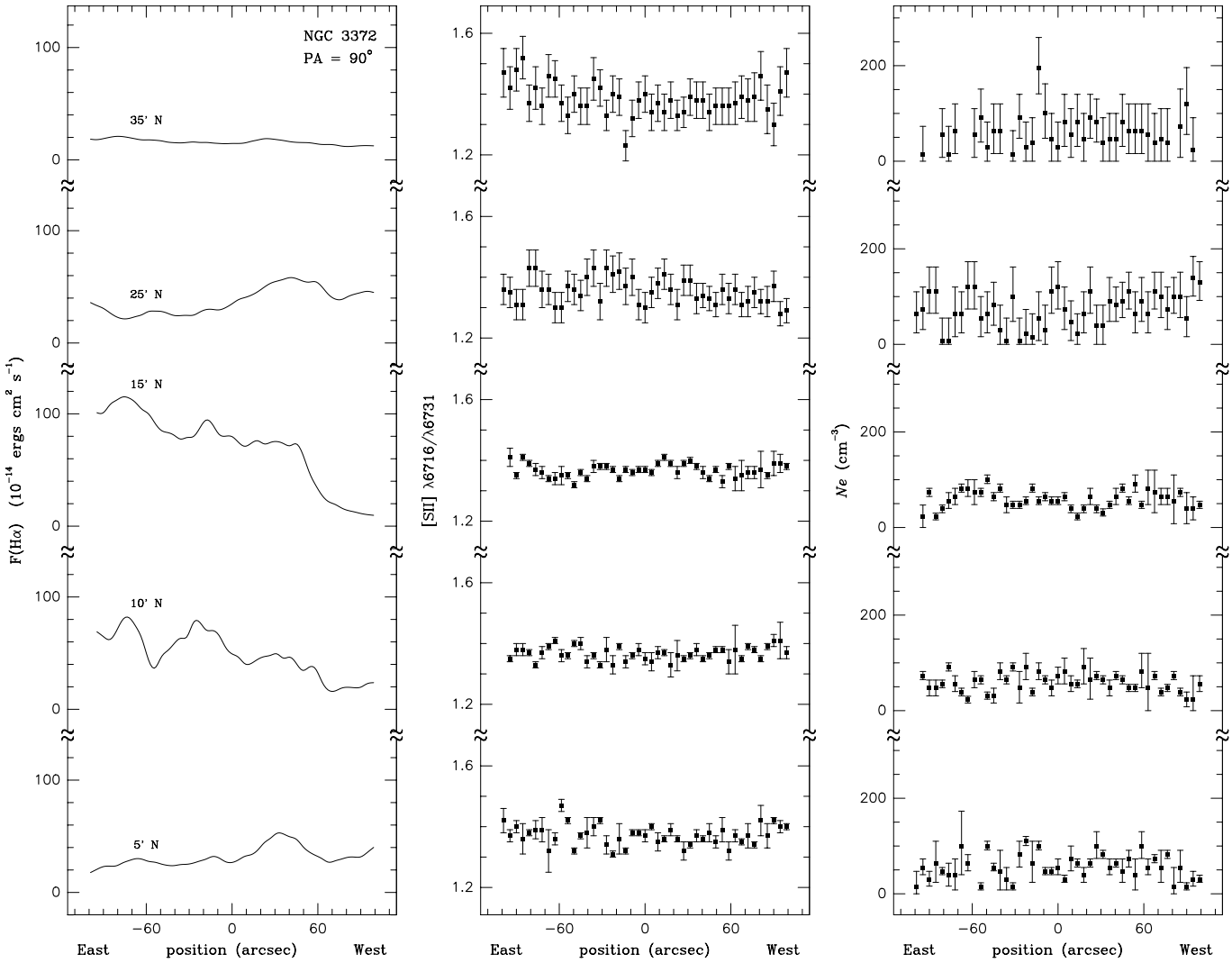

Fig. 14. NGC 3372 – The η Carina nebula, PA = 0°. Data profiles along the east-west direction. Positions are relative to the hour circle crossing η Car. The labels are the offsets in declination from this star. Other conventions as in Fig. 1

NH_3, CH_3OH and H_2O masers, Herbig-Haro objects, bipolar outflows and dense molecular clouds in the area (De Pree et al. 1995; Loughran et al. 1986; Persi et al. 1996; Rodríguez et al. 1982) shows that NGC 6334 is a rich cite of recent or even ongoing star formation, specially on the molecular ridge, roughly parallel to the galactic plane, that crosses the nebula.

Gum 62 and Gum 64a are two components of the NGC 6334 H II region complex (Maršálková 1973). The results for these objects are illustrated in Figs. 15 and 16. Gum 62 shows a well defined density gradient with a peak value of $N_{\rm e} = 490^{+41}_{-38}$ cm^{-3} at the Hα maximum. Gum 64a shows a similar density variation with the electron density reaching its maximum, $N_{\rm e} = 519^{+43}_{-39}$ cm^{-3}, on the region of sharp variation of the Hα profile and decreasing abruptly to the west and more gradually to the east. Right on the west side of Gum 64a there is an area of recent star formation revelled by the presence of OH and H_2O masers, a CO hot spot and a strong IR peak (Loughran et al. 1986; Rodríguez et al. 1982). The position of Gum 64a relative to these sources, its cone morphology and the detected density gradient may be explained by a 'champagne' flow in the nebula. The same phenomenon may also be responsible for the density gradient and the asymmetrical morphology of Gum 62. A study on the dynamics of these objects is necessary to confirm these suppositions.

4.12. M 20 – The Trifid nebula

On optical images M 20 appears as a bright and circular nebula trisected by prominent dark lanes (Lynds & O'Neil 1985). Radio observations disclose the near-spherical morphology of the Trifid nebula (Chaisson & Willson 1975). Our results (Figs. 17-20) reveal a systematic and relatively smooth variation of the electron density with position in this nebula with the density ranging from 100 to 300 cm^{-3}. The obscured region to the west of the central star coincides with the area of density enhancement. A density peak was also found at the position of the bright rim 25″ north of this star, corresponding to the narrow Hα peaks

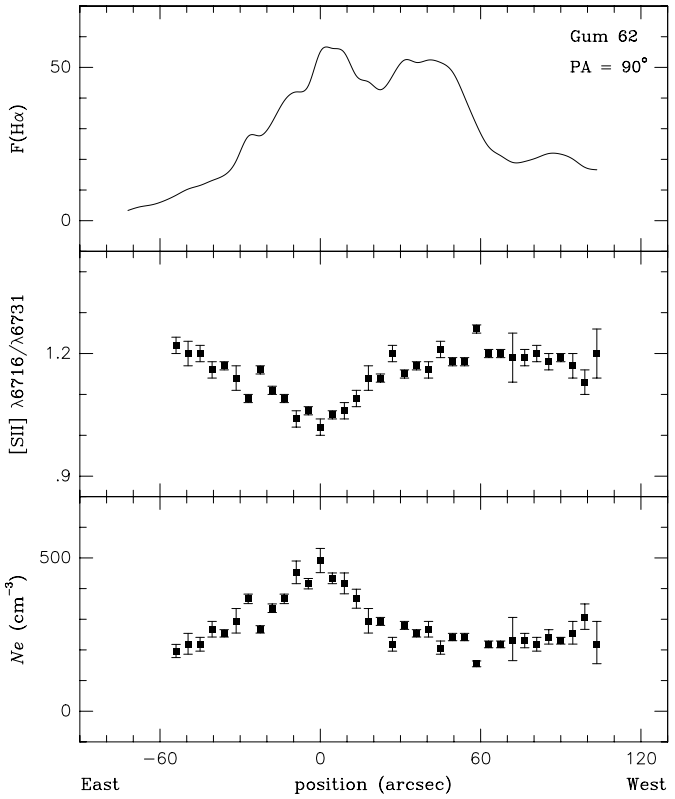

Fig. 15. Gum 62. Same as Fig. 1

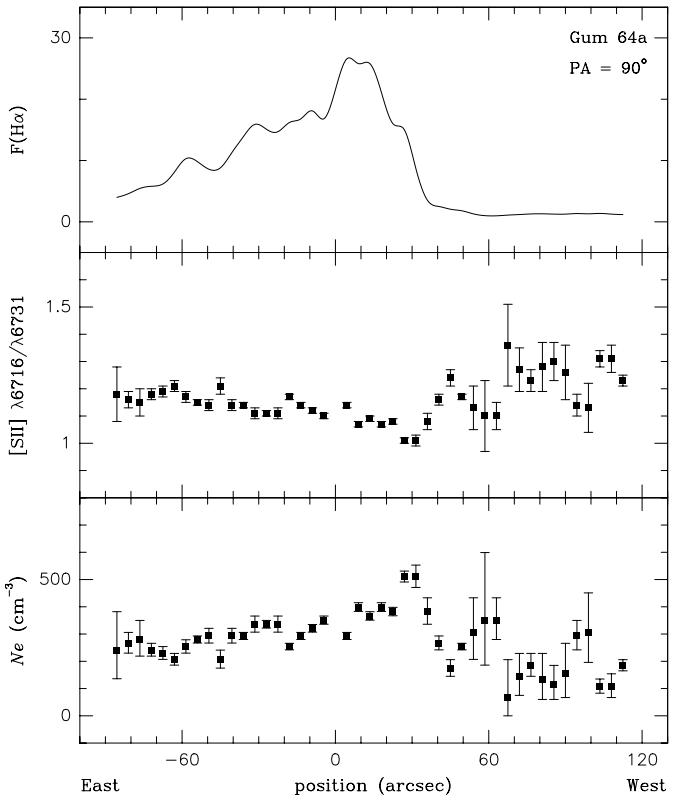

Fig. 16. Gum 64a. Same as Fig. 1

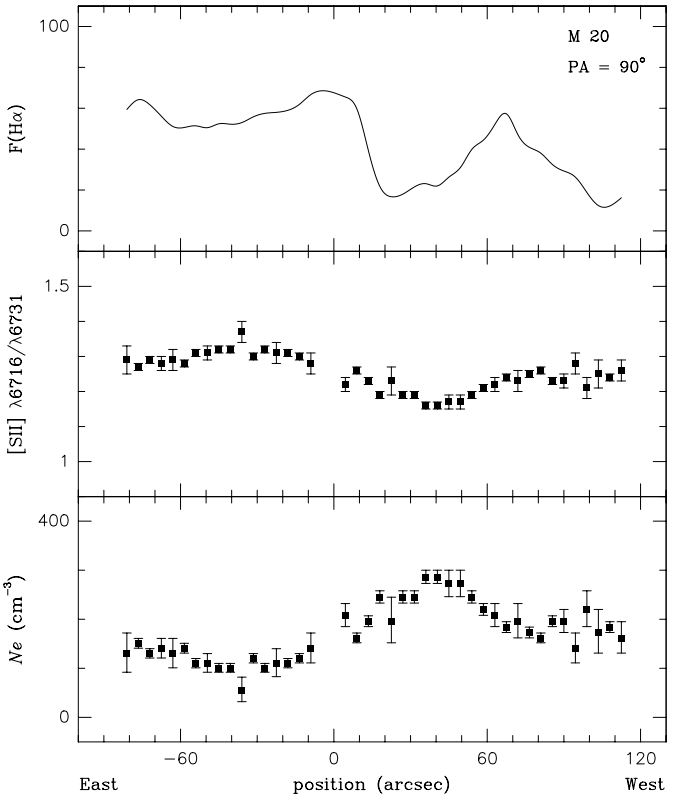

Fig. 17. M 20, the Trifid nebula, PA = 90°. Same as Fig. 1

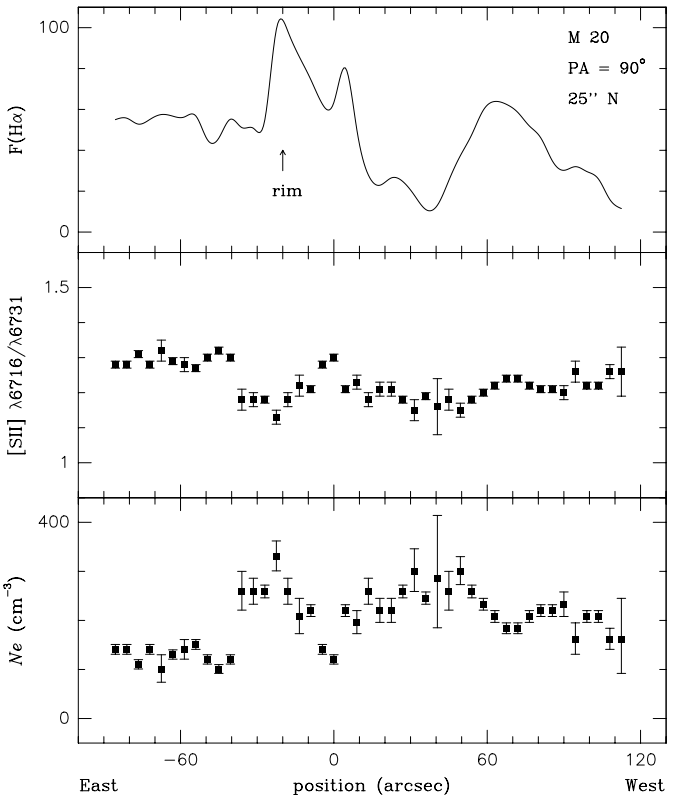

Fig. 18. M 20, the Trifid nebula, PA = 90°, $\Delta\delta = 25''$N. Same as Fig. 1

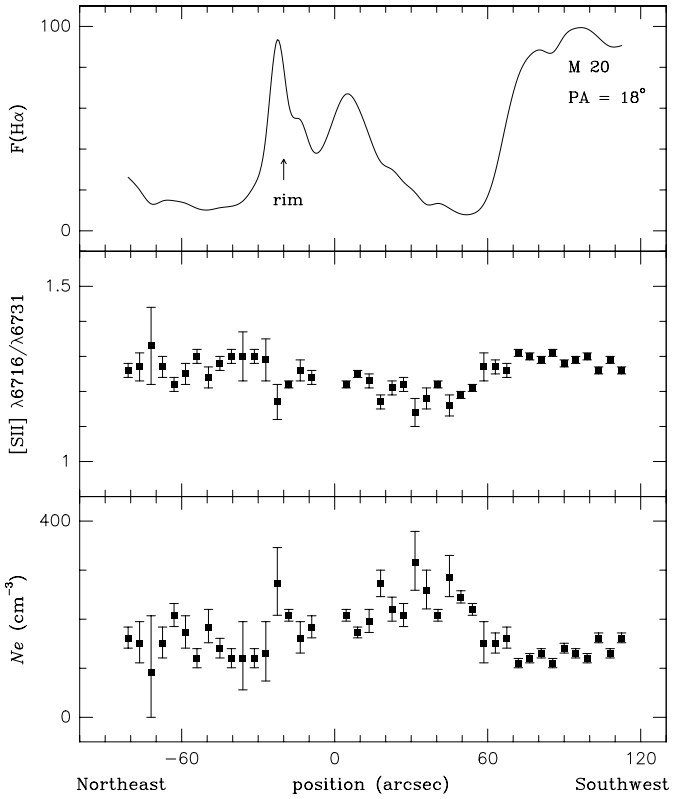

Fig. 19. M 20, the Trifid nebula, PA = 18°. Same as Fig. 1

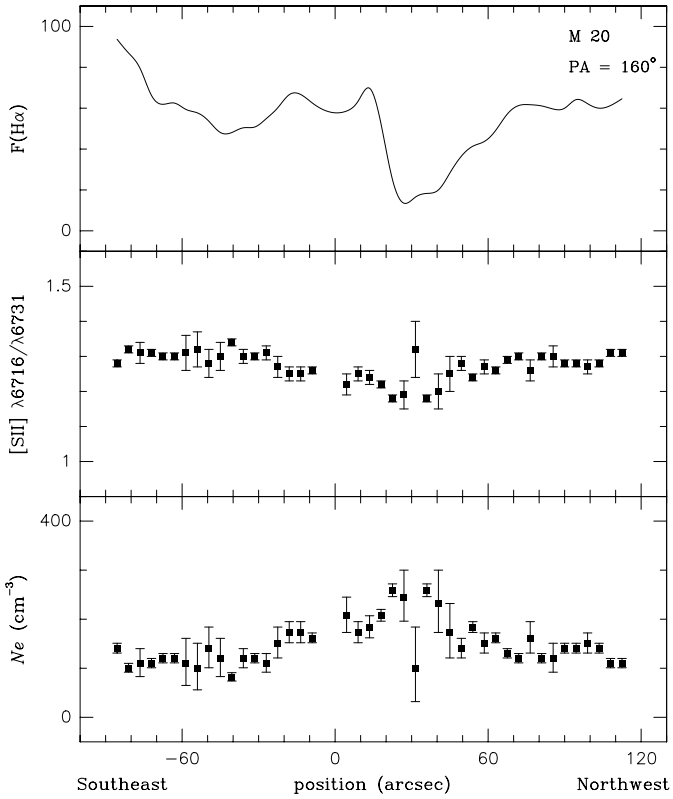

Fig. 20. M 20, the Trifid nebula, PA = 160°. Same as Fig. 1

indicated in Figs. 18 and 19. This filament is not resolved in our observations, so higher density values are expected in this region. Probably due to insufficient signal-to-noise, none of the two previous detailed studies on the variation of electron density in the Trifid nebula found in the literature (Bohuski 1973; Lynds & O'Neil 1985), based on photographic spectroscopy, have unveiled the spatial density distribution shown here. Bohuski (1973) have found mean densities from 400 to 800 cm^{-3} for most of the nebula and higher densities up to 6000 cm^{-3} on a bright rims near the southern edge of the nebula. Although these high density values obtained from an obsolete electron density calibration are not reproduced in the present work, we have a fairly good qualitative agreement with some of the results of Bohuski (1973) that have indicated lower densities in the region east of the central star, enhanced rim densities and higher densities near one of the absorption lanes. The average electron density of 230 $\pm$ 100 cm^{-3} and the more moderate density of 800 cm^{-3} for the northern bright rim obtained by Lynds & O'Neil (1985) are consistent with our results.

4.13. IC 1275

On the POSS prints this is a diffuse and roughly elliptical nebula. IC 1275 is the H II region of our sample with the lowest surface brightness. Fig. 21 shows that this object has also the lowest electron density with a mean value of $N_{\rm e}$ = 17^{+20}_{-17}, In many positions we have obtained [S II] ratios on the low-density limit.

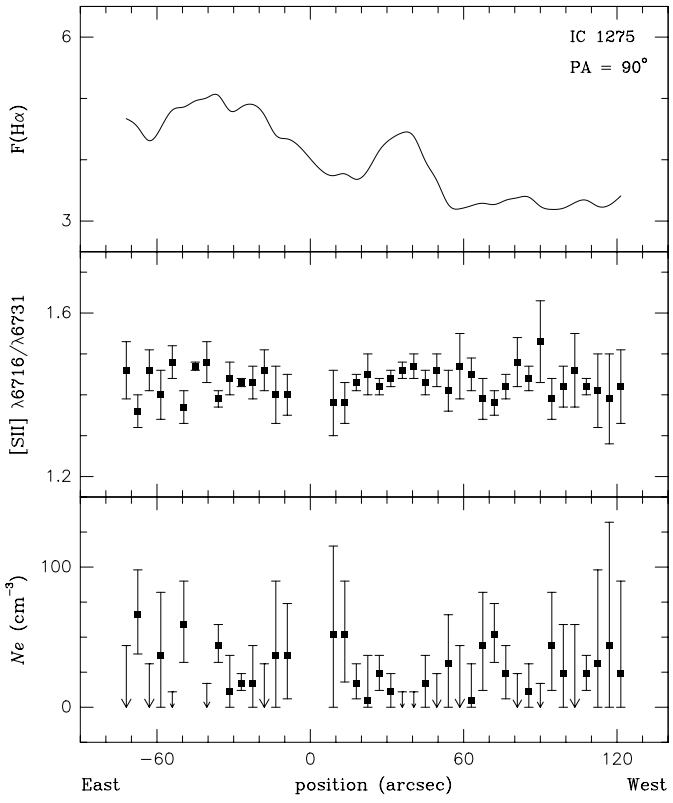

Fig. 21. IC 1275. Same as Fig. 1

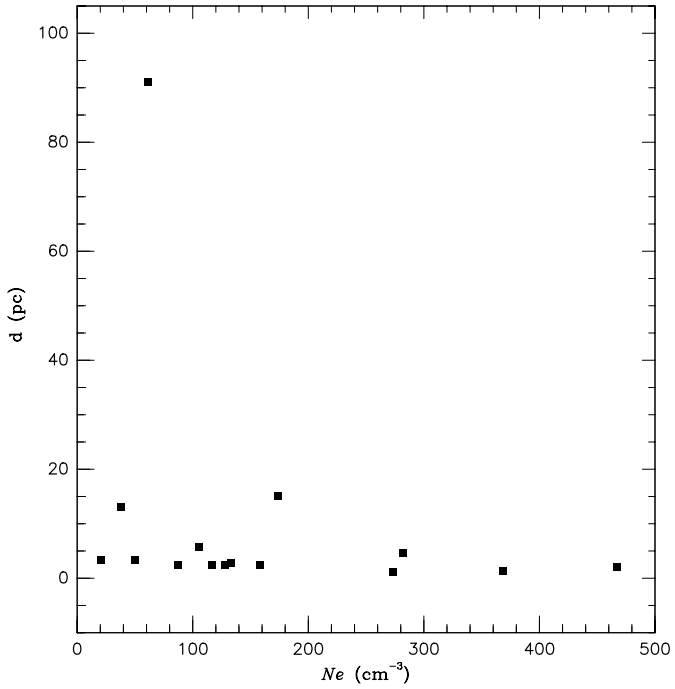

Fig. 22. Diameter vs. mean electron density

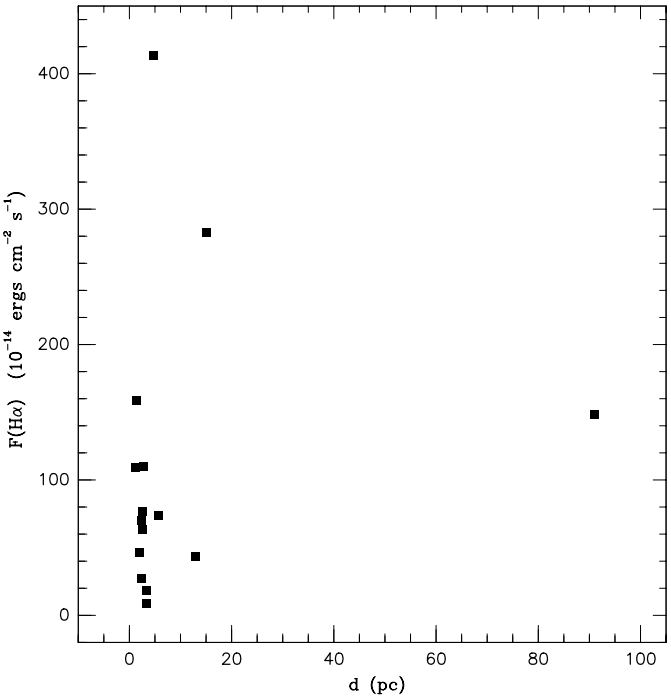

Fig. 23. Mean Hα flux vs. diameter

5. Discussion and conclusions

We have derived electron densities across 15 galactic H II regions from [S II] ratios measured through long-slit spectrophotometry with unprecedently high signal-to-noise. All the objects but the giant Carina nebula ($\sim$ 91 pc) are classical H II regions ($\sim$ 2–15 pc). Dense and compact or ultra-compact H II regions with sizes of tenths of parsecs associated with very young stellar objects were not included in our sample.

We have not detected any systematic spatial variation of electron density in nearly half of the objects studied (S 255, S 257, S 271, S 285, S 301, S 305, NGC 3372 and IC 1275). They are in general the most diffuse and probably evolved objects with low mean densities in the range $N_{\rm e} \approx$ 20–140 cm^{-3}. In some cases, this uniform distribution may be apparent due to the fact that the [S II] ratios are close to the low density limit. The remaining objects (S 288, S 307, NGC 2579, NGC 3503, Gum 62, Gum 64a and M 20) with mean densities $N_{\rm e} \approx$ 80–360 cm^{-3}, have shown a statistically significant electron density dependence on position. In most of the cases, the spatial variation of density may be interpreted as a radial gradient with the density decreasing from the centre to the edges.

With the exception of NGC 2579 with a peak density of $N_{\rm e} \approx$1700 cm^{-3}, the observed objects present low mean electron densities of the order of $N_{\rm e} \approx$20–360 cm^{-3}. These densities are consistent with the typical values obtained for giant extragalactic H II regions. So, in general the classical galactic H II regions are not readily distinguished from their giant extragalactic counterparts in terms of electron density. The very high values of electron density up to 6000 cm^{-3} reported in the literature for some of the objects studied here were not confirmed by our observations. In most of the cases the discrepancy should be accounted on the use of out-of-date atomic parameters.

It is important to stress that the [S II] ratio is a density indicator for the more external zones of the H II regions, so higher density in the inner parts were not directly discarded by our observations. However, since the S^+ ionisation zone occupies a large fraction of the total volume of a low excitation H II region, substantial amount of very high density gas are not expected in the observed objects excepting NGC 2579. Therefore, the present work supports the common assumption that classical and evolved H II regions generally have low electron densities, so that collisional de-exitation processes play a minor role.

In many objects of the sample, the zones of maximum surface brightness correspond to the zones of maximum density, specially in those objects showing indications of a central density gradient (e.g. S 288, S 307, NGC 2579, NGC 3503). In others, local density peaks are found associated to bright rims or filaments (e.g. M 20, NGC 3372). On the other hand, some objects show brightness fluctuations not matched by density variations. In fact, the extinction corrected Hα flux from an area of an H II region, corresponding to a solid angle of $d\Omega$, is given by

$$F(\mathrm{H}\alpha) = \frac{d\Omega}{4\pi} h\nu_{\mathrm{H}\alpha}\, \alpha_{\mathrm{H}\alpha} \int N_{\rm e}^2 \phi\, ds,$$

where $\alpha_{\mathrm{H}\alpha}$ is the effective recombination coefficient for Hα. So, brightness fluctuations with position may due to electron density, nebular depth or filling factor variations or even due to irregular dust extinction across the nebula. Taking the mean values of density and Hα flux in order to characterise each object, we have plotted in Figs. 22-24 the electron density, Hα

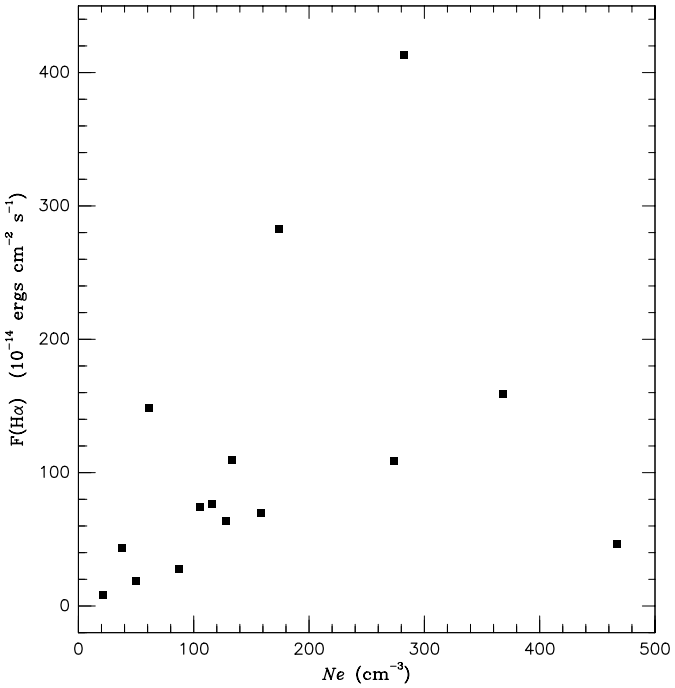

Fig. 24. Mean Hα flux vs. mean electron density

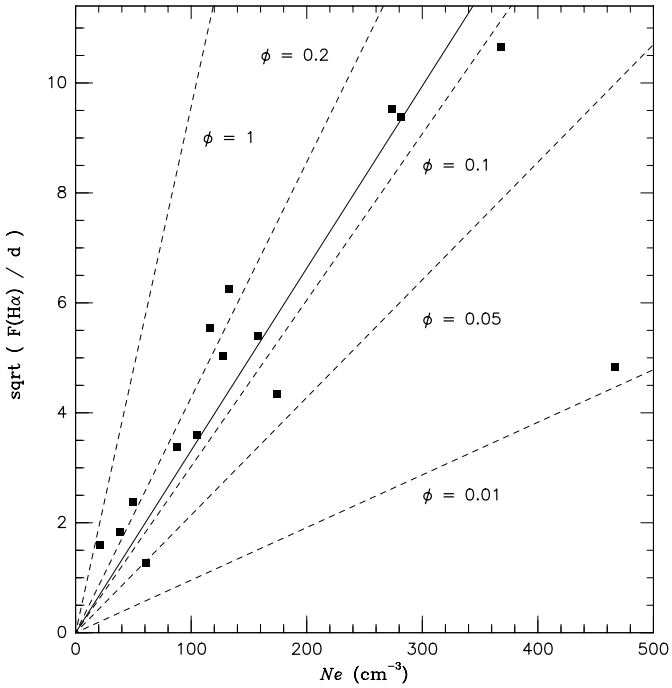

Fig. 25. The square root of $F(\mathrm{H}\alpha)/d$ vs. mean electron density. The dashed lines correspond to the expected relationship of these parameters in a homogeneous nebula for five different values of filling factor ϕ = 1, 0.2, 0.1, 0.05 and 0.01. The solid line is the regression line and corresponds to ϕ = 0.12

flux and diameter against one another. No individual relationship between any two of these properties was perceived. Yet, the expected relationship among them,

$$F(\mathrm{H}\alpha) \propto N_{\mathrm{e}}^2 \phi\, d,$$

is clearly depicted in Fig. 25, which shows that $\sqrt{F(\mathrm{H}\alpha)/d}$ correlates remarkably well with N_{e} with a correlation coefficient of R = 0.96, indicating a limited range of values for the fourth variable involved, the filling factor. In this figure, we have also shown that a nebular clumping corresponding to a mean filling factor of the order of ϕ = 0.1 is compatible with our data. The object NGC 2579 is the single outlier in this plot. Since both the distance and the extinction correction for this object are uncertain due to its unconfirmed identification with the complex RCW 19/20, an independent determination of this properties should be made before any further discussion.

The anti-correlation observed between rms electron density and diameter (Habing & Israel 1979; Kennicutt 1984) may reflects the decrease of the filling factor with size at least for non-compact and evolved objects with sizes of 2 to 100 pc across.

The only object in the sample with previously reported clear indications of 'blister' or 'champagne flow' effects, S 307, has revealed to present an electron density gradient in accordance with these models. Since systematic density variations of this sort are characteristic of this dynamical phenomenon, we suggest that NGC 2579, Gum 62, Gum 64a and possibly NGC 3503 are good candidates of showing a 'champagne effect'. Kinematical studies of these nebulae are necessary to confirm this indication.

Acknowledgements. This work was partially supported by the Brazilian institutions CNPq and FAPERGS. We thank the anonymous referee for very helpful comments and suggestions.

References

Albert C.E., Schwartz P.R., Bowers P.F., Rickard L.J., 1986, AJ 92, 75
Azcarate I.N., Cersosimo J.C., Colomb F.R., 1987, Rev. Mex. Astron. Astrofis. 15, 3
Azcarate I.N., Cersosimo J.C., Colomb F.R., 1990, Rev. Mex. Astron. Astrofis. 20, 23
Azcarate I.N., 1991, Ap&SS 180, 105
Bohuski T.J., 1973, ApJ 184, 93
Bowen I.S., 1960, ApJ 132,1
Buscomb W., 1963, Mount Stromlo Mimeographs, No. 7
Castañeda H.O., Vilchez J.M., Copetti M.V.F., 1992, A&A 260, 370
Caswell J.L., Haynes R.F., 1987, A&A 171, 261
Chaisson E.J., Willson R.F., 1975, ApJ 199, 647
Chopinet M., Deharveng-Baundel L., Lortet-Zuckermann M.C., 1974, A&A 30, 233
Chopinet M., Lortet-Zuckermann M.C., 1976, A&AS 25, 179
Deharveng L., Maucherat M., 1975, A&A 41, 27
De Pree C.G., Rodríguez L.F., Dickel H.R., Goss W.M., 1995, ApJ 447, 220
De Robertis M.M., Dufour R.J., Hunt R.W., 1987, J. R. Astron. Soc. Can. 81, 195
Feinstein A., 1995, Rev. Mex. A&ASC 2, 57
Felli M., Churchwell E., 1972, A&AS 5, 369
Felli M., Harten R.H., 1981, A&A 100, 42
Fich M., 1993, ApJS 86, 475
Fich M., Silkey M., 1991, ApJ 366, 107
Georgelin Y.P., Georgelin Y.M., 1970, A&AS 3, 1
Gum C.S., 1955, Mem. R. Astron. Soc. 67, 155
Habing H.J., Israel F.P., 1979, ARA&A 17, 345
Hawley S.A., 1978, ApJ 224, 417

Herbst W., 1975, AJ 80, 212
Herbst W., Miller D.P., Warner J.W., Herzog A., 1982, AJ 87, 98
Hunter D.A., 1992, ApJS 79, 469
Israel F.P., 1976, A&A 52, 175
Israel F.P., 1978, A&A 70, 769
Janes K., Adler D., 1982, ApJS 49, 425
Kazes I., Walmsley C.M., Churchwell E., 1977, A&A 60, 293
Kennicutt R.C., 1984, ApJ 287, 116
Keenan F.P., Hibbert A., Ojha P.C., Conlon E.S., 1993, Phys. Scr. A 48, 129
Kilian-Montenbruck J., Gehren T., Nissen P.E., 1994, A&A 291, 757
Lada C.J., Wooden D., 1979, ApJ 232, 158
Lahulla J.F., 1987, AJ 94, 1062
Lo K.Y., Burke B.F., 1973, A&A 26, 487
Loughran L., McBreen B., Fazio G.G., et al., 1986, ApJ 303, 629
Lynds B.T., Canzian B.J., O'Neil E.J., 1985, ApJ 288, 164
Lynds B.T., O'Neil E.J., 1985, ApJ 294, 578
LyngåG., Hansson N., 1972, A&AS 6, 327
Maršálková P., 1973, Ap&SS 27, 3
Matthews C.L., 1981, ApJ 245, 560
McCall M., 1984, MNRAS 208, 253
McCall M.L., Rybski P.M., Shields G.A., 1985, ApJS 57, 1
McGee R.X., Newton L.M., 1981, MNRAS 196, 889
Meaburn J., 1969, Ap&SS 3, 600
Moffat A.F.J., Fitzgerald M.P., Jackson P.D., 1979, A&AS 38, 197
Nakano M., Kogure T., Mizuno S., et al., 1983, Ap&SS 89, 407
Neckel T., 1978, A&A 69, 51
Neckel T., Staude H.J., 1995, ApJ 448, 832
Osterbrock D., Flather E., 1959, ApJ 129, 26
Peimbert M., Torres-Peimbert, S., Rayo J.F., 1978, ApJ 220, 516
Perek L., Kohoutek L., 1967, Catalogue of galactic planetary nebulae. Academia Prague
Persi P., Ferrari-Toniolo M., Shivanandan K., Spinoglio L., 1987, A&AS 70, 437
Persi P., Roth M., Tapia M., et al., 1996, A&A 307, 591
Pişmiş P., Hasse I., 1976, Ap&SS 45, 79
Ramsbottom C.A., Bell K.L., Stafford R.P., 1996, ADNDT 63, 57
Reifenstein III E.C., Wilson T.L., Burke B.F., Mezger P.G., Altenhoff W.J., 1970, A&A 4, 357
Rodgers A.W., Campbell C.T., Whiteoak J.B., 1960, MNRAS 121, 103
Rolleston W.R.J., Dufton P.L., Fitzsimmons A., 1994, A&A 284, 72
Rubin R.H., 1989, ApJS 69, 897
Rudolph A.L., Simpson J.P., Haas M.R., 1997, ApJ 489, 94
Rodríguez L.F., Cantó J., 1982, ApJ 255, 103
Russeil D., Georgelin Y.M., Georgelin Y.P., Le Coarer E., Marcelin M., 1995, A&AS 114, 557
Sabbadin F., Hamzaoglu E., 1981, A&A 94, 25
Saraph H.E., Seaton M.J., 1970, MNRAS 148, 367
Sharpless S., 1959, ApJS 4, 257
Shaver P.A., 1969, MNRAS 142, 273
Shaver P.A., McGee R.X., Newton L.M., Danks A.C., Pottasch S.R., 1983, MNRAS 204, 53
Silverglate P.R., Terzian Y., 1979, ApJS 39, 157
Smartt S.J., Dufton P.L., Rolleston W.R.J., 1996, A&A 310, 123
Tapia M., Roth M., Marraco H., Ruiz M.T., 1988, MNRAS 232, 661
Tenorio-Tagle G., 1979, A&A 71, 59
Turbide L., Moffat A.F.J., 1993, AJ 105, 1831
Turner K.C., Terzian Y., 1985, AJ 90, 59
Vílchez J.M., Esteban C., 1996, MNRAS 280, 720
Vorontsov-Velyaminov B.A., 1953, Gasnebel und neue Sterne. Berlin
Walborn N.R., 1973, AJ 78, 1067
Walborn N.R., 1982, AJ 87, 1300
Wilson T.L., Mezger P.G., Gardner F.F., Milne D.K., 1970, A&A 6, 364
Wouterloot J.G.A., Brand J., 1989, A&AS 80, 149
Zijlstra A., Pottasch S., Bignell C., 1990, A&AS 82, 273